IOPscience iopscience.iop.org

Home Search Collections Journals About Contact us My IOPscience

Structures and molecular dynamics of solution-grown and melt-grown samples of n-heptatriacontane

This article has been downloaded from IOPscience. Please scroll down to see the full text article.

1996 J. Phys.: Condens. Matter 8 5301

(http://iopscience.iop.org/0953-8984/8/29/007)

View the table of contents for this issue, or go to the journal homepage for more

Download details:
IP Address: 171.66.16.206
The article was downloaded on 13/05/2010 at 18:20

Please note that terms and conditions apply.

J. Phys.: Condens. Matter **8** (1996) 5301–5316. Printed in the UK

Structures and molecular dynamics of solution-grown and melt-grown samples of n-heptatriacontane

J Fenrych, E C Reynhardt and I Basson

Department of Physics, University of South Africa, PO Box 392, Pretoria 0001, South Africa

Received 1 September 1995

Abstract. The crystal structures and molecular dynamics of solution-grown and melt-grown polycrystalline samples of n-heptatriacontane have been investigated by employing NMR, DSC and x-ray powder diffraction techniques. The solution-grown sample has an orthorhombic structure, while the melt-grown sample is a mixture of a monoclinic and an orthorhombic structure. Three relaxation mechanisms are present in all samples, namely, threefold reorientation of methyl groups, defect motions of chain-ends between all-*trans* and defect orientations and twofold chain reorientations. In the high-temperature phases an additional relaxation process due to translational–rotational diffusion of chains is present.

1. Introduction

Polymorphism of n-alkanes, n-C_nH_{2n+2} (abbreviated as C_n) with $n \geqslant 30$, has been investigated by a number of authors [1–7]. The four polymorphic forms which have been reported for C_{36} include an orthorhombic modification (OI), with chains parallel to the *c* axis, and the unit cell comprising four chains from two adjacent layers [1]. A different orthorhombic form (OII), in which chains are inclined with respect to the plane of chain-ends, was described by Khoury *et al* [2] and Kobayashi *et al* [3]. The *c* cell dimension of the OII structure can be obtained from the *c* cell dimension of the OI structure by multiplying the latter by $\cos\psi$, where $\psi = 12.4^\circ$ is the inclination angle of the chains with respect to the normal to the plane of chain-ends. Sullivan and Weeks [4] proposed different monoclinic structures, which can be derived from the OI structure. For example, the carbon atom positions in the M_{011} structure [5] can be obtained from the OI unit cell by translating each $–CH_2–$ unit of the adjacent chain along the *b* axis by four $–CH_2–$ units parallel to the *c* axis. The chains are inclined with respect to the methyl end-group plane at an angle of 62.8°. The subscript is the Miller subcell index of the plane formed by the terminal methyl groups. Another monoclinic form, M_{201}, was recently reported for melt-crystallized C_{36} [6]. A wide range of n-alkanes (C_{32} to C_{80}) was studied by Takamizawa *et al* [7] with special emphasis on the purity of the samples. All these n-alkanes exhibited a high-temperature monoclinic phase. The M_{101} structure was observed for shorter chains ($n < 45$) and M_{201} for longer ones. M_{011} and OI structures, or mixtures of these structures, were observed for (C_{48}) at room temperature, depending on the solvent and conditions of crystallization.

Sirota *et al* reported five rotator phases for n-alkanes, ranging from C_{16} to C_{33} [8]. R_I and R_{II} coincide with the rotator phases reported earlier by Ungar [20], while R_{IV} and R_V are related to the high-temperature monoclinic phases observed by Sullivan and Weeks [4] and Takamizawa *et al* [7]. The R_{III} rotator phase has triclinic symmetry.

0953-8984/96/295301+16$19.50 © 1996 IOP Publishing Ltd

The interpretation of low-angle x-ray diffraction, IR spectroscopy and proton second moment measurements of uniaxially oriented C_{33} by Strobl *et al* [9] and Ewen *et al* [10] led to the conclusion that each solid–solid phase transition is linked to the onset of a specific motion. It was proposed that at the first solid–solid phase transition ($A \rightarrow B$) rotational jumps of chains in the all-*trans* conformation about their long axes are activated, followed by the introduction of translations of chains in the logitudinal direction at the $B \rightarrow C$ transition. Interchain defects occur only in the high-temperature rotator phase *D*. Using infrared techniques, Maroncelli *et al* [11, 12] observed the presence of chain defects in the vicinity of the rotator phase and reported the probabilities of their occurrence in n-alkanes of different chain lengths. Ueda *et al* [13] measured the proton spin–lattice relaxation time in the dipolar field for C_{50} and obtained an activation energy of 42 kJ mol^{-1} for rotational diffusion in a solution-crystallized sample and a very high activation energy of $\sim$ 150 kJ mol^{-1} for translational–rotational diffusion in a melt-crystallized sample. Employing ^{13}C CPMAS, Jarret *et al* [14] observed *trans–gauche* conformational disorder at chain-ends in melt-crystallized C_{60}. In addition, it was proposed that the rotational and longitudinal motions are activated at the solid–solid phase transition.

In a recent NMR investigation of a series of n-alkanes ranging between C_{22} and C_{28}, Basson and Reynhardt [15] proposed a model in which fast defect motions of chain-ends between all-*trans* and $gtg't_{m-3}$ defect orientations dominate proton spin–lattice relaxation in the rotating frame in the temperature range 200–330 K. The experimental data were explained in terms of an asymmetric double potential well for the two conformations.

In this paper an investigation of the molecular dynamics and phase changes of a medium length n-alkane, C_{37}, employing DSC, x-ray powder diffraction and proton spin–lattice relaxation time measurements, is reported. It forms part of a research project in which the structures and molecular dynamics of n-alkanes and mixtures of n-alkanes, with chain-lengths between 36 and 48 carbon atoms, are investigated.

2. Experimental details

The C_{37} sample with stated purity of $> 98\%$ was obtained from Fluka GmbH and was used without further purification. Three samples were investigated. Sample 1 was recrystallized from a saturated solution in C_8 by decreasing the temperature at a rate of about 1.5 K h^{-1} from 320 K to room temperature (295 K). Sample 2 was obtained from sample 1 by heating it to phase *C* (345 K) and allowing it to cool to room temperature (295 K). Sample 3 was crystallized from the melt at a cooling rate of about 5 K min^{-1}. DSC thermograms were recorded on a Standton Redcroft DSC700 instrument. Samples of about 5 mg were heated at a rate of 1 K min^{-1} in open aluminium pans in a nitrogen atmosphere.

X-ray spectra were recorded on a Seifert MZIV diffractometer using Cu Kα radiation and a Ni filter. Diffractograms were obtained in three 2θ intervals, namely 3° to 10°, 20° to 25° and 35° to 42°. The width of the detector slit was 0.01 mm and the temperature was controlled with an accuracy of about 1 K. With a view to limiting preferential orientation, polycrystalline samples were ground to fine powders in a mortar and pestle, immersed in a liquid nitrogen bath to reduce the plasticity of the samples.

Proton spin–lattice relaxation times were measured on a Bruker CXP200 spectrometer and a home-made spectrometer operating at 75 MHz. The pulse sequences for T_1 and $T_{1\rho}$ measurements have been described elsewhere [6].

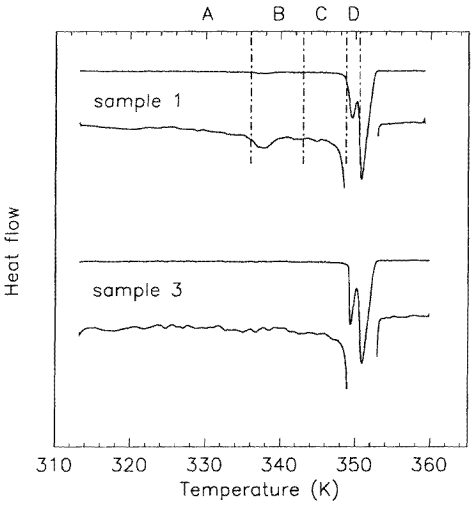

Figure 1. DSC thermograms of samples 1 and 3. The lower trace for each sample has a ten times higher sensitivity.

3. Results

3.1. DSC

The DSC thermogram obtained for sample 1 is shown in figure 1. It exhibits a solid–solid phase transition with the onset at about 335 K and another one at about 349 K, followed by the peak of the melting transition at 350 K. Between the two solid–solid transitions a wide slightly endothermic region, which does not exhibit a peak, is observable. Takamizawa *et al* [7] reported two solid–solid phase transitions at about 333 K ($A \rightarrow B$) and about 342 K ($B \rightarrow C$), as well as the transition to the rotator phase D, the latter overlapping with the melting transition. Although the $B \rightarrow C$ transition is not observable on our DSC thermogram, a gradual change of the x-ray diffractogram in the 2θ range between 3° and 10° starts in the vicinity of 342 K. Therefore, the same phase notation will be used in the rest of the discussion. At a later stage the absence of a DSC peak in the vicinity of 343 K will be explained in terms of conclusions drawn from the x-ray results. Also shown in figure 1 is the DSC thermogram obtained for sample 3. The solid–solid phase transition at 335 K is absent for this sample.

3.2. X-ray powder diffraction

X-ray powder diffractograms for sample 1, obtained at several temperatures in the 2θ ranges mentioned in section 2, are shown in figure 2. Above 340 K each of the low-angle diffraction peaks consists of two superimposed lines. With a view to obtaining the exact positions and relative intensities of the superimposed lines, two Gaussian-shaped lines were fitted to the unresolved diffraction peak at $2\theta \approx 7.5^\circ$ by treating the amplitudes, half-widths and peak positions as variable parameters. Figure 3 displays the temperature dependences of the lamellar thickness L and the a and b cell dimensions for samples 1 and 2. The presence of two a dimensions above 325 K will be explained in section 5.1. Diffractograms for samples 1 and 2 are compared in figure 4(a). Two diffractograms for sample 3, obtained at

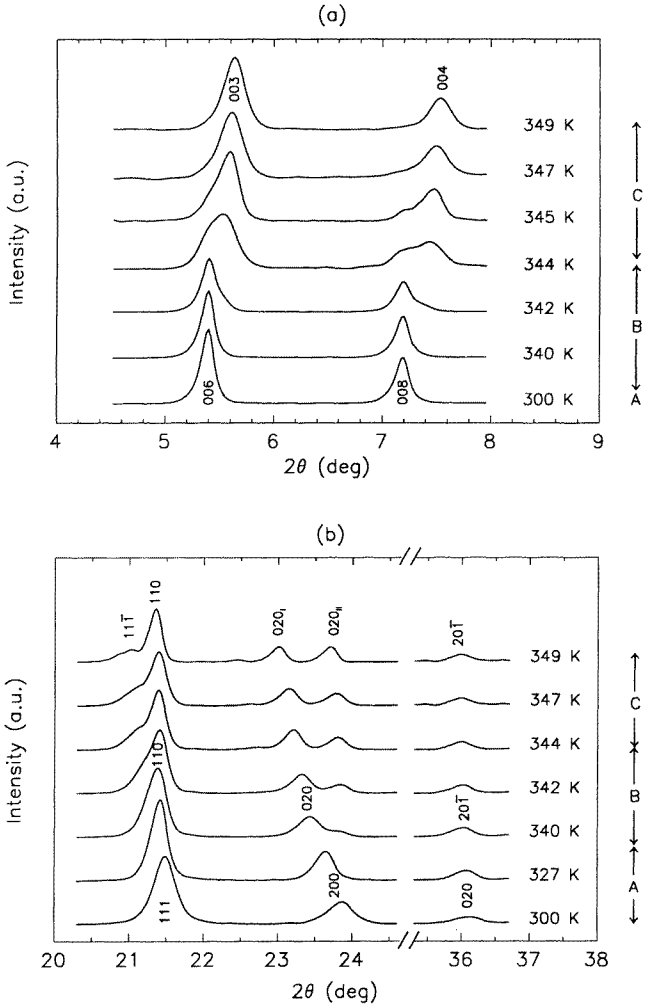

Figure 2. Diffractograms for the solution-grown sample 1 as a function of temperature. Different solid phases are indicated by the symbols A, B and C.

different time intervals after preparation, are shown in figures 4(b) and (c).

With a view to explaining the observed diffraction patterns, the Rietveld program [16] was used to simulate diffractograms of the orthorhombic OI and OII structures and all the monoclinic structures. The carbon atom coordinates for the OI and M_{110} unit cells, listed by Teare [1] and Shearer and Vand [5], respectively, were used. The unit cells of M_{012}, M_{101}, M_{201} and OII were obtained by applying the transformations described by Sullivan and Weeks [4] and Kobayashi *et al* [3]. The simulated diffractograms have already been reported for C_{36} [6].

3.3. NMR relaxation

The temperature dependences of T_1 for samples 1 and 3, measured at 75 and 200 MHz, are shown in figure 5. Both samples reach a minimum at $\beta \approx 6.0\ \mathrm{K}^{-1}$ ($\beta \equiv 1000/T$) for

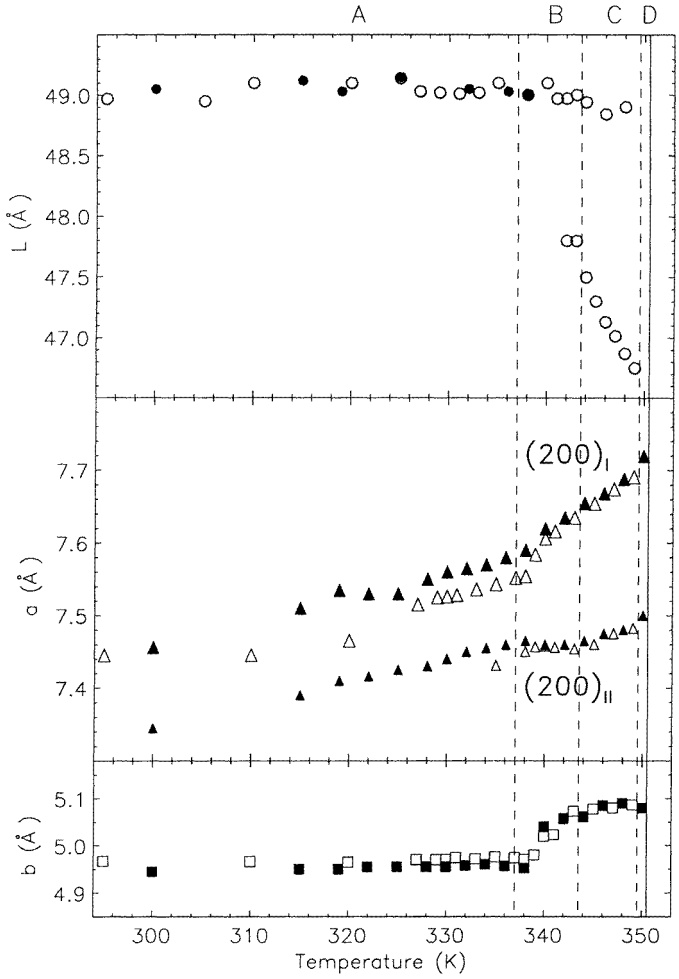

Figure 3. Temperature dependence of lamellar thickness (L) and a and b cell dimensions for sample 1 (open symbols) and sample 2 (solid symbols). For the a dimension two sets of data, corresponding to two (200) peaks are shown.

$\omega_0/(2\pi) = 200$ MHz, but the curve for sample 3 is shifted towards higher temperatures. The temperature dependence of $T_{1\rho}$ for samples 1, 2 and 3, measured in a rotating field of 15 G (1 G $\equiv 10^{-4}$ T), is displayed in figure 6. In sample 1 for $\beta < 5$ K^{-1}, $T_{1\rho}$ decreases with increasing temperature but a minimum cannot be identified with confidence prior to the first solid–solid phase transition. In phases B and C an abrupt increase of $T_{1\rho}$ was observed. For sample 2 a $T_{1\rho}$ minimum was observed at $\beta \approx 3.1$ K^{-1}. Sample 3 exhibits a slightly deeper minimum which is shifted towards lower temperatures.

In the temperature range between the melting point ($\beta = 2.85$ K^{-1}) and $\beta = 3.9$ K^{-1} the decay of the magnetization with increasing length of the spin-locking pulse was found to be non-exponential for samples 1 and 2. In this temperature range two relaxation times

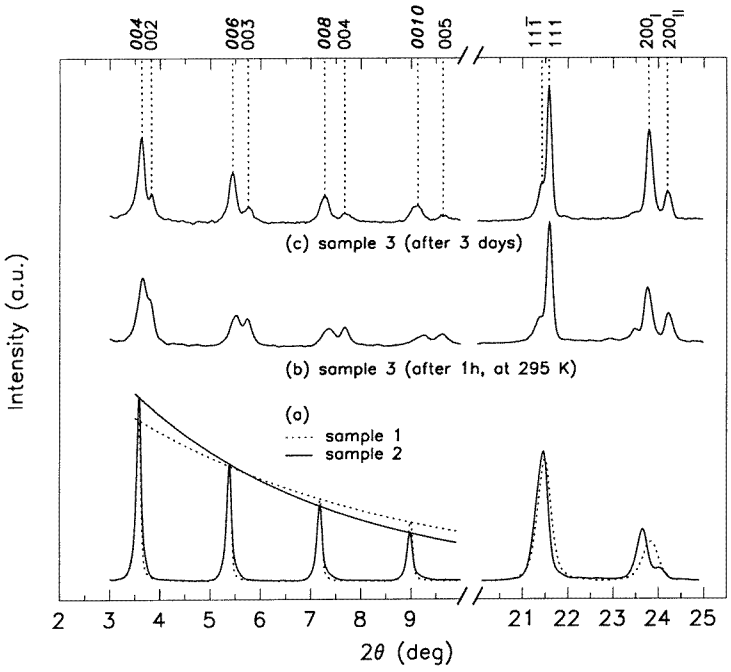

Figure 4. Observed diffractograms for sample 2 at 300 K (a) and sample 3 at 295 K (b) and (c). For $2\theta < 10^\circ$ the lower angle peaks correspond to the orthorhombic structure. The diffractogram of sample 1 at 295 K is shown as a dotted line. The envelopes of the decaying peak intensities are also shown.

were isolated by using the equation

$$\frac{M}{M_0} = \left[Q \exp\left(\frac{-\tau}{T_{1\rho s}}\right) + (1-Q)\exp\left(\frac{-\tau}{T_{1\rho \ell}}\right)\right] \tag{1}$$

where M_0 and M are the magnetization at $t = 0$ and $t = \tau$ respectively. $T_{1\rho s}$ and $T_{1\rho \ell}$ are the short and long relaxation times, respectively. Q is the fraction of the protons relaxing at the faster rate. Sample 3 exhibited exponential decay of the magnetization (see figure 7).

4. Summary of relevant theory

The proton spin-lattice relaxation rate in the laboratory frame for a threefold methyl group reorientation is given by [17]

$$T_1^{-1} = \tfrac{2}{3}\gamma^2 \Delta M_2 [J(\omega_0) + 4J(\omega_0)] \tag{2}$$

where $J(\omega_0)$ is the spectral density function

$$J(\omega_0) = \frac{\tau_c}{1+\omega_0^2\tau_c^2} \tag{3}$$

and τ_c the correlation time for the proton jump, described by the Arrhénius formula

$$\tau_c = \tau_0 \exp\left(\frac{E_a}{RT}\right). \tag{4}$$

ΔM_2 is the proton second moment reduction and ω_0 the Larmor frequency.

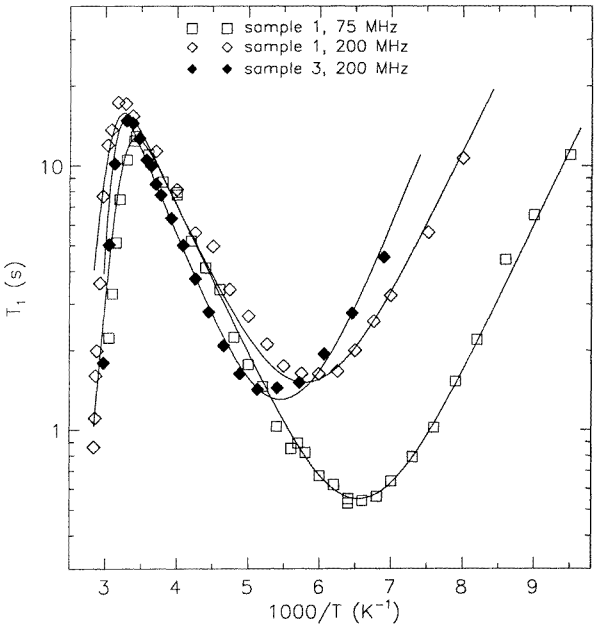

Figure 5. Spin–lattice relaxation times in the laboratory frame as a function of inverse temperature for samples 1 and 3. Solid lines are best fits of equation (2) to the experimental data.

The spin–lattice relaxation rate in the rotating frame for the same reorientation is [17]

$$T_{1\rho}^{-1} = \tfrac{2}{3}\gamma^2 \Delta M_2 (\tfrac{3}{2} J(2\omega_1) + \tfrac{5}{2} J(\omega_0) + J(2\omega_0)) \tag{5}$$

where the angular frequency associated with the rotating field is given by $\omega_1 = \gamma H_1$. If a pair of protons jumps between two orientations A and B with different potential energies, the populations of the two orientations are unequal and the relaxation rate is increased. For such a model the relaxation rate in the rotating frame is given by [18]

$$T_{1\rho}^{-1} = \tfrac{2}{3}\gamma^2 \Delta M_2 \frac{4a}{(1+a)^2} (\tfrac{3}{2} J(2\omega_1) + \tfrac{5}{2} J(\omega_0) + J(2\omega_0)) \tag{6}$$

where a, the relative probability p_A/p_B of occupation of the two orientations, is given by

$$a = \exp\left(\frac{\Delta E}{RT}\right). \tag{7}$$

ΔE is the energy difference between the two orientations and ΔM_2 is the second moment reduction if $a = 1$.

5. Discussion

5.1. X-ray powder diffraction

5.1.1. Sample 1. The observed diffractogram of sample 1 at 300 K (figure 2) reveals the orthorhombic OI structure with cell dimensions $a = 4.97 \pm 0.01$ Å, $b = 7.45 \pm 0.01$ Å and $c = 98.1 \pm 0.1$ Å. The lamellar thickness ($L = c/2$) is 49.05 $\pm$ 0.1 Å, in agreement with the value of 48.97 Å, calculated by Broadhurst [19]. While heating sample 1, L remains

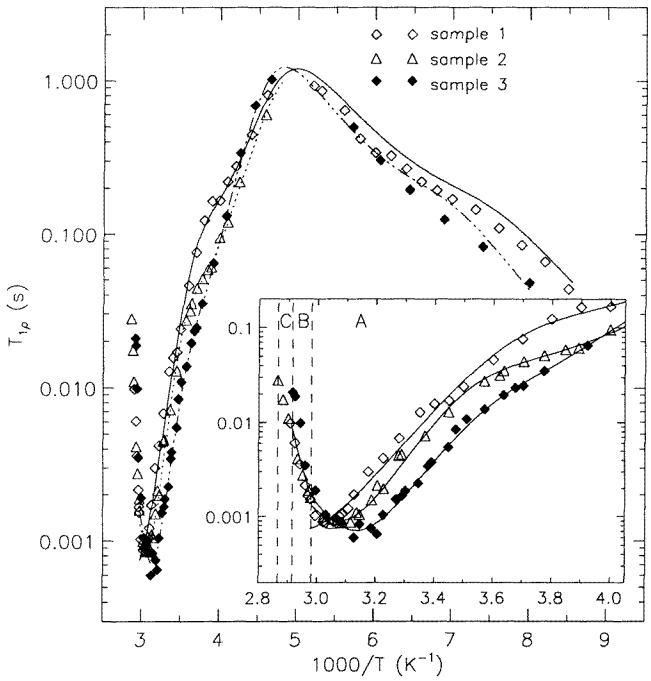

Figure 6. Spin–lattice relaxation times in the rotating frame as a function of inverse temperature for samples 1, 2 and 3. Solid lines are best fits of equations (5) and (6) to the experimental data.

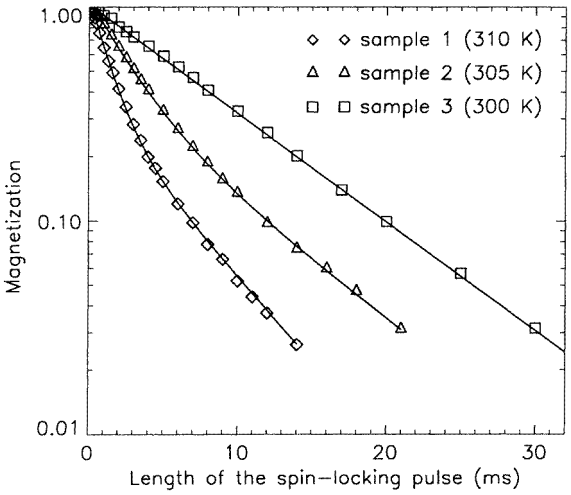

Figure 7. Examples of $T_{1\rho}$ relaxation curves for samples 1, 2 and 3. Solid lines are best fits of equation (1) to the experimental data.

constant up to the phase transition $B \rightarrow C$ (figure 3). The *a* dimension increases gradually with increasing temperature, while the *b* dimension remains almost constant up to 340 K.

At about 337 K the expansion coefficient of the *a* cell dimension changes significantly, characterizing the $A \rightarrow B$ phase transition. This phenomenon was also reported by Strobl *et al* [9] and Takamizawa *et al* [7]. Begining at 342 K, a second structure with $L \approx 47.8$ Å starts to grow at the expense of the original orthorhombic structure. Simultaneously small shifts of the peaks in the range $20^\circ > 2\theta > 35^\circ$ are observable (figure 2(b)). Indexing of the peaks at 342 K with orthorhombic space groups $Pbca$ or $Pca2_1$ gives unsatisfactory results. However, if a monoclinic unit cell with space group $P\,2_1/c$ is considered, good agreement is obtained with the observed peaks indexed as (110), (020) and $(20\bar{1})$. An additional shoulder appearing on the low-angle side of the (110) peak is indexed as $(11\bar{1})$. The β angle calculated from the positions of these peaks increases gradually in phase *B* and reaches the value of about 104° at 343 K. For the sake of simplicity, the interchange between the *a* and *b* cell dimensions in going from the OI (orthorhombic) to the M_{012} (monoclinic) structure will be ignored and thus peaks indexed as (020) in phases *B* and *C* will be treated as (200).

At the transition $B \rightarrow C$ the intensities of the (00ℓ) diffraction peaks associated with the new phase (shorter lamellar thickness) increase dramatically (see figure 2(a)), while those of the orthorhombic phase decrease. At 347 K the intensity ratio of the peaks of the two phases is about 10:1. A decrease of the long spacing at the $B \rightarrow C$ transition was also observed by Takamizawa *et al* [7], but the presence of two structures was not reported. Their calculation of the inclination angle of the chains with respect to the plane of the end groups indentified the M_{101} monoclinic stucture in phase *C* (calculated long spacing of 46.4 Å). In the present investigation this value is not observed, even at temperatures close to the melting point. The shorter long spacing of 47.5 Å obtained at 344 K could be an indication that the $B \rightarrow C$ transition is to the M_{012} rather than to the M_{101} structure. The β angle calculated from the position of the $(11\bar{1})$, (110), (020) and $(20\bar{1})$ peaks is also in close agreement with the value of 104.4° predicted for the M_{012} structure [4].

The Rietveld simulation of a mixture of structures consisting of 10% OI and 90% M_{012} resolves the observed diffractogram satisfactorily with the exception of one peak appearing at $2\theta \approx 24^\circ$ in phase *B*. A similar phenomenon was encountered for melt-crystallized C_{36} [6]. Since the low-angle diffractogram showed the coexistence of three structures, it was proposed that the shoulder at the high-angle side of the (200) peak could be assigned to a (020) peak of the monoclinic structure. In the present study this phenomenon was investigated in more detail. The peak appearing at $2\theta \approx 24^\circ$ was indexed as $(200)_{II}$ and the temperature dependence of the *d*-spacings and intensities of the $(200)_I$ and $(200)_{II}$ peaks (figure 2(b)) were determined by fitting two Gaussian-shaped lines to the partially resolved peaks. Figure 3 shows the *a* cell dimensions thus obtained, while figure 8 shows the temperature dependence of the intensities of these peaks. It is clear that the weak $(200)_{II}$ reflection is already present in phase *A*, but a significant increase in its intensity takes place in phase *B*. However, in the same temperature range the intensity of the $(200)_I$ peak does not change significantly. The origin of the structure with the shorter *a* dimension needs further discussion.

The two structures identified by the splitting of the (200) peak are related to domains with different planar conformers. The expansion of the *a* cell dimension, related to an increase of the *d*-spacing of the $(200)_I$ peak, was discussed by Ungar [20] and Doucet *et al* [21, 22] for odd n-alkanes ranging from C_{17} to C_{25} and Takamizawa [7] for C_{33} and C_{45}. This phenomenon is related to a hindered reorientation of chains along their long axis. In C_{23} and C_{25} a hexagonal symmetry is reached for which $a = \sqrt{3}b$ and chains rotate freely. Monte Carlo simulations of rotator phases by Yamamoto [23] revealed the presence of ordered domains of size about 30 Å within which the chains tend to parallel their zigzag

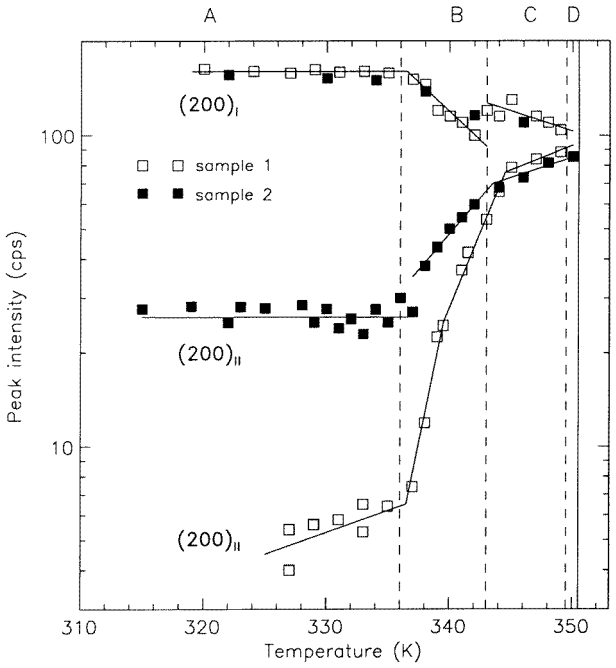

Figure 8. Temperature dependence of peak intensities of the two (200) peaks for sample 1 and sample 2.

planes. Thus the $(200)_I$ peak originates from domains of stretched chains reorienting about their long axes.

On the other hand, defect reorientations seem to result in domains consisting of unit cells with the shorter *a* dimension. Chain defects create obstacles to the rotation of chains. In such domains the interlayer zone is disordered but the rest of the layer is not affected and forms a more tighly packed structure than the one with rotating chains. Maroncelli *et al* [11, 12] found that in phase *C*, the average *gauche* fraction for C_{29} at the second C–C bond is about 3%, implying that 6% of the molecules have defects at chain ends. The probability of finding defects in chains increases with increasing chain length [11] and it is expected that for C_{37} approximately about 20% of the chains are in end-*gauche* conformations. gtg' kinks are also highly populated in phase *C* [11]. In section 5.1.2 a method for evaluating the interlayer disorder is discussed and the result clearly shows that a number of end-defects and gtg' kinks are present in phase *C* at 345 K. NMR results show the presence of chain-end defect motions already in the ordered phase *A* prior to chain reorientations about the long axis. The model discussed in section 4 implies that the population of chain-end defects increases with temperature according to the Boltzmann distribution. From equation (7) and the NMR results listed in table 2, it is estimated that the population of chain-end defects in phase *B* is about 18%. If the rotational and conformational disorder is combined, the domain model with different local dynamics can account satisfactorily for all obseved phenomena.

In solution-crystallized C_{36} chain reorientations are absent and only defect motions are present [6]. The x-ray results of C_{36} are consistent with the model outlined above. A splitting of the (200) peak was not observed and the expansion of the *a* dimension was smaller than for the domains with rotational disorder in C_{37} ($a = 7.72$ Å below the melting

Table 1. Estimated parameters of the interface region for samples 1 and 2.

	T [K]	d_{av}(Å)	d_s(Å)	D_t(Å)
Sample 1	295	1.82	1.85	2.6
	345	1.88	1.82	8.3
Sample 2	315	2.00	1.90	5.4

Table 2. Motional parameters for the reorientations in the different phases of C_{37}.

Sample	Type of reorientation	E_a (kJ mol^{-1})	τ_o (s)	ΔM_2 (G^2)	ΔE (kJ mol^{-1})
Sample 1	Threefold CH_3 reorientation	10.6 ± 0.8	$(2.9 \pm 0.2) \times 10^{-13}$	1.3 ± 0.1	
	Chain-end defect motion	21 ± 1	$(5.3 \pm 0.2) \times 10^{-11}$	1.0[a]	12.0 ± 0.5
	Twofold chain reorientation	62 ± 2			
Sample 2	Chain-end defect motion	21 ± 1	$(2.0 \pm 0.2) \times 10^{-11}$	1.0[a]	10.0 ± 0.5
	Twofold chain reorientation	78 ± 2	$(1.9 \pm 0.2) \times 10^{-19}$	10.0[a]	7.0 ± 0.5
Sample 3	Threefold CH_3 reorientation	12.6 ± 0.8	$(1.3 \pm 0.2) \times 10^{-13}$	1.4 ± 0.1	
	Chain-end defect motion	31 ± 1	$(1.1 \pm 0.2) \times 10^{-12}$	1.0[a]	9.5 ± 0.5
	Twofold chain reorientation	76 ± 2	$(2.2 \pm 0.2) \times 10^{-19}$	10.0[a]	6.0 ± 0.5

[a] Calculated values.

point). The a dimension of 7.54 Å reported for C_{36} before the melting transition is closer to the a dimension of the domains with conformational disorder in C_{37} where $a = 7.49$ Å below the melting transition. The appearence of an additional peak in the 2θ range between 20° and 24° in phase C was also reported by Strobl *et al* for C_{33}, but an explanation for this phenomenon was not offered.

Heating in phase C results in a gradual decrease of the shorter L-spacing (figure 3). Since the β angle remains constant in phase C at about 104°, a gradual change in the inclination angle can be ruled out. A possible explanation is that the chains are effectively shortened by an increase in the number of chain defects.

5.1.2. Sample 2. Sample 2 has the OI structure at 300 K (the lamellar thickness is approximately the same as for sample 1 in phase *A*), but a number of interesting phenomena differentiate it from sample 1. Firstly, the $(200)_{II}$ peak, although only a shoulder on the high-angle side of the $(200)_I$ peak, is observable, even at 300 K, as shown in figure 4(a). The temperature dependence of its position is similar to that observed for the $(200)_I$ peak. Its intensity is almost temperature independent in the low-temperature phase up to the transition to phase *B*, where an abrupt increase is observed, similar to what was observed during the heating of sample 1 (figure 8). Secondly, the geometry of the *a*–*b* plane has changed slightly, as can be seen from figure 3. The *a* dimension is slightly larger, while the *b* dimension is slightly smaller. However, the area of the *a*–*b* plane is almost unchanged, 37.45 Å^2 for sample 1 and 37.50 Å^2 for sample 2. Finally, the decay of the intensities of the (00ℓ) peaks with increasing ℓ is faster for sample 2 than for sample 1, as shown in figure 4(a).

With a view to investigating changes in chain packing, the model proposed by Strobl *et al* [9] was employed. Three parameters describing the lamellar interface were estimated for sample 1 at 295 K and 345 K and for sample 2 at 315 K. These parameters, illustrated in figure 9, are d_s the thickness of the plain layer of voids separating adjacent lamellae, which

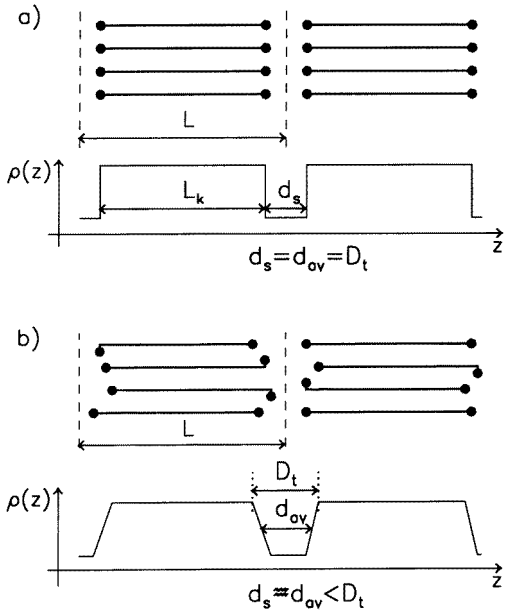

Figure 9. Schematic representation of (a) ordered and (b) disordered lamellar structures with the corresponding electron density distributions $\rho(z)$ in the direction of the molecular axes.

is given by the difference between the lamellar thickness L and the length of a stretched chain, L_k, projected onto the normal to the surface, d_{av} the average local thickness of the void layer and D_t, the overall thickness of the interface region. The parameters listed in table 1 were obtained by considering the first five (00ℓ) peaks.

In order to compare the experimental results with possible changes in the interlamellar space due to configurational disorder, a calculation was made for a sample with 25% of the chains in an all-*trans* configuration, 55% of the chains with an end-*gauche* configuration and 20% of the chains with gtg' configuration (20%). Translations of chains were included to retain the tight packing in the middle zone of the chains. In such a system d_{av} increases approximately by 30% while D_t increases by a factor of three when compared with an ordered structure.

From the experimental results it is clear that D_t for sample 1 increases by a factor of four in going from 295 K to 345 K, implying that disorder in the interlayer space is probably slightly higher than estimated earlier. The small increase of d_{av}, as compared with sample 1 at 295 K, is an indication that the tight packing in the middle of the chain is retained.

For sample 2, D_t is almost three times as large as d_{av}. This result suggests that the cooling of sample 1 from phase *C*, thus forming sample 2, introduces disorder into the interface region. It seems that the chain-end disorder gets frozen into the structure. This is in agreement with an earlier assumption which relates the appearance of the $(200)_{II}$ peak at $2\theta \approx 24^\circ$ to chain-end defects. Strobl *et al* [9] indicated that the increase of D_t in phases *B* and *C* was due to the translation of chains in the longitudinal direction, but did not consider the effect of chain-end defects. In phase *D* the activation of interchain defects in the middle of the chain was proposed as an explanation for the increase in the average local thickness d_{av} and D_t of the order of 10 Å.

5.1.3. Sample 3. One hour after melting sample 1 and recrystallization to form sample 3, two different long spacings of about 48.1 Å and 46.2 Å were observed (figure 4(b)) A diffractogram recorded three days later for the same sample reveals the same pattern, but the peaks of the shorter L-spacing are less intense, while the longer L is slightly longer at about 48.5 Å (figure 4(c)). The structure with the longer L-spacing is OI, (calculated $L = 48.98$ Å [19]), while the other structure is probably M_{101} since both the long spacing and the angle β calculated from the (110) and (111) peak positions are in agreement with the predicted values [4]. It is significant that the strong $(200)_{II}$ peak is present, yielding a shorter a dimension of 7.35 Å. Reynhardt *et al* [6] showed that C_{36} recrystallized from the melt consists of three phases, namely OI, OII and M_{201}, the fractions of the different structures being a function of the cooling rate. When the cooling rate was about 5 K min^{-1}, the OI structure was predominant, while very slow recrystallization (about 1 K h^{-1}) yielded predominantly OII and M_{011} structures. It was also reported that in the orthorhombic structure the population of defects frozen into the structure is high, while monoclinic structures favour all-*trans* chains. The present investigation shows that the composition of C_{37} recrystallized from the melt at a fast cooling rate changes with time. The OI structure grows at the expense of the monoclinic structure. It is to be expected for odd-numbered n-alkanes, for which the lowest energy conformation is orthorhombic, while the monoclinic structures are metastable. In contrast, when C_{36} is crystallized slowly from the melt, the stable structure is monoclinic [6].

5.2. Spin–lattice relaxation in the laboratory frame

The T_1 minima of samples 1 and 3 are associated with threefold reorientation of methyl groups [15]. Best fits of equation (2) to the experimental data are shown as solid lines in figure 5 and the associated motional parameters are listed in table 2. The activation energy for this reorientation is slightly higher in sample 3 than in sample 1. It seems that in sample 3 the interfacial region contains end-*gauche* conformations, leading to higher barriers for methyl group reorientations. This phenomenon was also observed in the case of C_{36} [6]. Second moment reductions of 1.3 ± 0.1 G^2 for sample 1 and 1.4 ± 0.1 G^2 for sample 3, obtained from best fits to the experimental data, are in agreement with the calculated value of 1.3 G^2 for the reorientation of an isolated methyl group.

5.3. Spin–lattice relaxation in the rotating frame

5.3.1. Non-exponential $T_{1\rho}$ relaxation. The non-exponential relaxation showed in figure 7 could be assigned to a number of sources. Melt-crystallized C_{36} [6] has two separate spin systems, corresponding to two crystallographic modifications. The short and long $T_{1\rho}$ values form two minima at different temperatures. In melted polyethylene [24], heterogeneity was due to different parts of the polymer chain, namely a slowly relaxing system of tight tubes and a region of fast isotropic reorientations of the chain-ends. If spin diffusion is not fast enough to provide fast cross-relaxation between these different parts, bi-exponential relaxation is observed.

More complex systems, such as liquid crystals and glass forming molecules, show strong deviations from exponential relaxation. Frequently the relaxation data are fitted with the Kohlrausch stretched exponential function [26], given here for the decay of magnetization:

$$M(t) = M(t = 0) \exp\left[-\left(\frac{t}{T_{1\rho}}\right)^{\beta}\right]. \tag{8}$$

Böhmer *et al* [25] compared more than 70 glass formers studied by a number of experimental techniques and showed a correlation between the parameter β and the so-called 'fragility' of a sample. The 'fragility' represents a deviation from the Arrhénius formula (equation (4)) in cases where the relaxation rates reveal very high activation energies. In these cases the Arrhénius formula yields a non-physical value of τ_0 and the more general Vogel–Fulcher formula is used to deal with this problem [27]. The explanation of the non-exponential behaviour in these compounds has usually been given in terms of (i) a spatially heterogeneous distribution of correlation times due to different clusters of molecules with different relaxation rates (parallel processes), or (ii) a serial process of non-exponential loss of correlation in a homogeneous system. The latter is usually explained as resulting from cooperative motions. Schmidt-Rohr and Spiess [28] investigated poly(vinyl acetate) by 2D and 'reduced 4D' exchange C^{13} NMR spectroscopy in order to determine the source of the observed non-exponential correlation function. It was shown that the segmental chain motion in this polymer is limited to clusters with different correlation times. The lifetime of a cluster was less than one second and thus the system was homogeneous on the time scale of a second.

For C_{37} equations (1) and (8) were fitted to the decay of the magnetization in the rotating frame. Equation (1) gave a slightly better fit to the experimental data, suggesting that a number of parallel processes influence the relaxation. The β parameter of the Kohlrausch equation proved useful in judging the deviation from exponential relaxation. It appeared that in phases *B* and *C* the non-exponentiality was stronger ($\beta \approx 0.6$) than in phase *A* ($\beta \approx 0.8$), in agreement with the domain model based on the x-ray results. Most probably some heterogeneity of chain motion exists in phase *A* due to the formation of domains with slightly different relaxation times. In phases *B* and *C*, two types of domains, with fast and slow reorienting chains, exist.

In sample 3 ($\beta \approx 0.9$) the heterogeneity is limited. On the other hand, two crystallographic modifications are present, suggesting that the chain dynamics in the orthorhombic and monoclinic forms are similar.

In order to extract the motional parameters from the temperature dependence of $T_{1\rho}$, the weighted average of the two relaxation times obtained from equation (1) is used. Cuthnell and Venable [29] followed the same approach in calculating the motional parameters of methyl group rotation in dimethyl sulphone, where cross-relaxation led to non-exponential spin–lattice relaxation.

5.3.2. Sample 1. It is clear that at least three relaxation mechanisms contribute to $T_{1\rho}$ in the region under investigation. The decrease of $T_{1\rho}$ in the region $\beta > 5\ K^{-1}$ is associated with the methyl group reorientation. The motional parameters for this motion have already been determined (table 2).

The temperature dependence of $T_{1\rho}$ in the region $\beta < 5\ K^{-1}$ reveals that the relaxation is due to a superposition of two processes, one with a lower activation energy resulting in the shallow minimum of about 0.1 s and the other with a higher activation energy leading to a minimum shorter than 1 ms which was not reached due to the $A \rightarrow B$ phase transition. Shallow $T_{1\rho}$ minima were observed by Basson and Reynhardt [15] for shorter n-alkanes in the same temperature region and ascribed to defect reorientations of chain-ends. C_{36} also showed such a shallow minimum [6]. The relaxation rate for such reorientations is given by equation (6). The calculated value of ΔM_2 is $1.0\ G^2$ [15]. For the experimental $T_{1\rho}$ data below $\beta \approx 3.5\ K^{-1}$ a fit of equation (6) was incorporated. However, only the activation energy of the reorientation influencing the relaxation in this temperature range is meaningful

since a minimum was not observed. This relaxation is most probably due to twofold chain reorientations.

In phase *B* the activation energy calculated from the slope of $T_{1\rho}$ versus β is 145 ± 5 kJ mol^{-1} and is similar to that reported by Ueda [13] for melt-crystallized C_{50}. Such a high energy could be explained if the translational–rotational diffusion of chains were considered rather than simple twofold reorientations.

5.3.3. Sample 2. The temperature dependence of $T_{1\rho}$ for sample 2 in the range $2.9 < \beta < 4.5$ K^{-1} is similar to that of sample 1. However, the deep minimum is shifted towards lower temperatures, which allows proper fitting of the theoretical model. The second moment reduction of 3.0 G^2 obtained from a fit of equation (6) to the experimental data with $\Delta E = 0$ is about one third the calculated value for twofold reorientations of chains, including both intra- and intermolecular contributions [15]. It is unlikely that the potential minima for a twofold reorientation of a chain in an n-alkane will be symmetrical. Implementation of an asymmetric potential well would lead to a shallower minimum, since the fraction $4a/(a+1)^2 < 1$ [18]. It follows from equation (6) that at high temperatures only a very small difference in energy between two orientations leads to a significant change in the depth of the $T_{1\rho}$ minimum.

For $\beta > 3.5$ K^{-1} the influence of defect motions on the relaxation time is more prominent than in the case of sample 1. A fit of equation (6) to the experimental data revealed that ΔE is slightly smaller than for sample 1. The resulting increase in the population of defect orientations in sample 2 is in agreement with the x-ray diffraction results which revealed the freezing of defect orientations into the orthorhombic structure.

5.3.4. Sample 3. The deep minimum which is due to chain reorientations is shifted towards lower temperatures, implying that the reorientation is faster at a given temperature in sample 3 than in samples 1 or 2. The activation energy for the chain reorientations is slightly higher than that for sample 1. However, the deeper minimum indicates a smaller ΔE value for sample 3. The effect of defect motions on the relaxation time is less prominent for this sample, implying that the minimum due to this reorientation is shifted towards higher temperatures. The fit of equation (6) to the experimental data reveals that this reorientation at a given temperature is faster for sample 3 than for samples 1 and 2. The theoretical curves are shown in figure 6 and the fitted parameters given in table 2.

5.4. DSC

Finally the absence of the endothermic peak at the the $B \rightarrow C$ transition must be addressed. It is surprising that the observed abrupt change in lamellar thickness is not reflected as an abrupt change in heat capacity. It is possible that translations of chains in the orthorhombic structure, which transform it to the monoclinic structure, are not triggered at one temperature, but that the transformation takes place over a wide temperature range. The coexistence of the OI and M_{012} structures in the range $342 < T < 349$ K supports this explanation.

6. Conclusions

The solution-grown sample of C_{37} has the orthorhombic structure OI. At 342 K the monoclinic structure M_{012} starts to grow at the expense of the OI structure. In the low-temperature phase, spin–lattice relaxation in the laboratory frame is dominated by threefold

reorientation of methyl groups, while the relaxation in the rotating frame is mainly influenced by defect motions of the chain-ends. In the high-temperature phases domains of stretched chains reorienting about their long axes and chains with conformational disorder at chain ends occur. When the solution-grown sample was heated to phase *C* and then cooled to room temperature, a higher degree of disorder was introduced into the interface region, and twofold chain reorientations could be isolated from the $T_{1\rho}$ relaxation data. The melt-grown sample is a mixture of the OI and M_{101} structures. The OI structure grows with time at the expense of the M_{101} structure. The chain reorientations occur at lower temperatures than in the solution-grown sample.

Acknowledgments

The Foundation for Research and Development and the Research and Bursaries Committee of the University of South Africa are thanked for financial support.

References

[1] Teare P W 1959 *Acta Crystallogr.* **12** 294
[2] Khoury F, Fanconi B, Barnes J D and Bolz L H 1973 *J. Chem. Phys.* **59** 5849
[3] Kobayashi M, Kobayashi T, Itoh Y, Chatani Y and Tadokoro H 1980 *J. Chem. Phys.* **72** 2024
[4] Sullivan P K and Weeks J J 1969 *J. Res. NBS* A **74** 203
[5] Shearer H M M and Vand V 1956 *Acta Crystallogr.* **9** 379
[6] Reynhardt E C, Fenrych J and Basson I 1994 *J. Phys.: Condens. Matter* **6** 7605
[7] Takamizawa K, Ogawa Y and Oyama T 1981 *Polymer J.* **14** 441
[8] Sirota E B, King H E Jr, Singer D M and Shao H H 1993 *J. Chem. Phys.* **98** 5809
[9] Strobl G, Ewen B, Fischer E W and Piesczek W. 1974 *J. Chem. Phys.* **61** 5257
[10] Ewen B, Strobl G and Richter R 1980 *Faraday Discuss. Chem. Soc.* **69** 19
[11] Maroncelli M, Strauss H L and Snyder R G 1985 *J. Chem. Phys.* **82** 2811
[12] Maroncelli M, Ping Qi S, Strauss H L and Snyder R G 19XX *J. Am. Chem. Soc.* **104** 6237
[13] Ueda T, Takeda S, Nakamura N and Chihara H 1991 *Bull. Chem. Soc. Japan.* **64** 1299
[14] Jarrett W L, Mathias L J, Alamo R G, Mandelkern L and Dorset D L 1992 *Macromolecules* **25** 3468
[15] Basson I and Reynhardt E C 1990 *J. Chem. Phys.* **93** 3604
[16] Rietveld H M 1968 *J. Appl. Crystallogr.* **2** 5
[17] Kubo R and Tomita K 1954 *J. Phys. Soc. Japan* **9** 888
[18] Andrew E R and Latanowicz L 1986 *J. Magn. Reson.* **68** 232
[19] Broadhurst M G 1962 *J. Res. NBS* A **66** 241
[20] Ungar G 1983 *J. Phys. Chem.* **87** 689
[21] Doucet J, Denicolo I and Craievich A 1981 *J. Chem. Phys.* **75** 1523
[22] Doucet J, Denicolo I, Craievich A and Collet A 1981 *J. Chem. Phys.* **75** 5125
[23] Yamamoto T 1985 *J. Chem. Phys.* **82** 3790
[24] Callaghan P T 1988 *Polymer* **29** 1951
[25] Böhmer R, Ngai K L, Angeli C A and Plazek D J 1993 *J. Chem. Phys.* **99** 4201
[26] Kohlrausch R 1854 *Pogg. Ann. Phys.* **91** 179
[27] Vogel H 1921 *Phys. Z.* **22** 645
Fulcher G S 1923 *J. Am. Ceram. Soc.* **8** 339
[28] Schmidt-Rohr K and Spiess H W 1991 *Phys. Rev. Lett.* **66** 3020
[29] Cutnell J D and Venable W 1974 *J. Chem. Phys.* **60** 3795